17.1 VLBI Phase Errors

In order to make aperture-synthesis images we must sample the amplitude and phase of the visibility at many points in the (u, v) plane and then Fourier invert and deconvolve the data (see chapter 1). Calibration of the visibility amplitude has been dealt with in chapter 9; in this chapter we discuss the calibration of the visibility phase. Visibility phase is defined to be the relative phase of the electric fields measured simultaneously at two points along the wavefront from the radio source. In practice however there will be a delay (the geometrical delay) between when the wavefront passes one antenna and when it passes the second antenna. There will also be additional delays due to passage through air and ionospheric plasma and through the electronics at each antenna, the sum of all these contributions being known as the total delay.

One of the functions of a correlator is to remove the effects of total delay using a delay model. However, inevitably, this model has a limited accuracy, $\Delta\tau(t)$. As a result, the visibilities generated by a correlator contain phase errors

$$\phi_{\rm corr}(t,\nu) = 2\pi\nu\Delta\tau(t) = 2\pi\Delta\ell(t)/\lambda\,,$$

where ν/λ is the observing frequency/wavelength, and $\Delta\ell = c\Delta\tau$ is the effective increase in propagation path length. This residual phase error $\phi_{\rm corr}(t,\nu)$ can be expressed as

$$\phi_{\rm corr}(t,\nu) = \phi_{\rm v}(t,\nu) + \phi_{\rm inst}(t,\nu) + \phi_{\rm geom}(t,\nu) + \phi_{\rm atmo}(t,\nu) + \phi_{\rm iono}(t,\nu)\,, \tag{17.1}$$

where $\phi_{\rm v}$ is the true visibility phase, $\phi_{\rm inst}$ is the sum of any residual instrumental phase errors at the two antennas (mainly due to the different frequency standards at each site), $\phi_{\rm geom}$ is the residual phase error due to geometric errors in the delay model and $\phi_{\rm atmo}$ and $\phi_{\rm iono}$ represent the effects of different neutral atmospheric and ionospheric delays above each antenna.

For VLBI data each of the terms in equation 17.1 is much larger and much more rapidly varying than for smaller connected-element (CE) arrays like the VLA. In practice, for VLBI observations $\phi_{\rm corr}$ can often change by a full turn over a few minutes or less (see figure 17.1*a*), and the phase errors can vary significantly over the bandpass, preventing an integration of the data over frequency. In this section we will examine the typical magnitudes of the path length errors, phase, delays and delay-rates introduced by each of the terms in equation 17.1.

17.1.1 Geometric Errors

Geometrical errors can be separated into two types; those caused by inadequate knowledge of the terrestrial coordinates of the antennas, and those due to errors in the assumed celestial coordinates of the source. We can consider terrestrial and celestial frames whose z axes are both defined by the earth's rotation axis. Errors in antenna positions relative to this rotation axis we classify as errors

in terrestrial coordinates while errors in source position vectors relative to this rotation axis we consider errors in celestial coordinates.

Errors in antenna coordinates can arise from:

1. Inaccurate antenna positions (which are typically known to $\approx$ cm-m); or ambiguities in combining together antenna coordinates measured in different terrestrial reference frames ($\approx$ m);

2. Movement of the antennas due to tectonic plate motion (in some cases of order $\approx$ cm yr^{-1}, e.g. the VLBA Mauna Kea antenna is expected to move $\approx$ 12 cm yr^{-1});

3. Polar motion, irregular and periodic shifts of the earth relative to its rotation axis of order $\Delta\theta = 100-500$ mas (Robertson, Carter and Fallon 1988);

4. Tidal effects due to lunar/solar gravitation, including solid earth tides (diurnal, $\approx$ 50 cm)

5. Ocean loading (diurnal, up to $\approx$ 3 cm 100 km from coast).

All these effects (and others) are discussed more fully in chapters 18 and 19; see also Sovers (1991). Antenna position errors give rise to errors in the assumed baseline vectors of amplitude $\Delta\vec{B}_\lambda$ (in wavelengths). The residual fringe-rate due to such a baseline error is of order $\omega\Delta\vec{B}_\lambda$, e.g. for a baseline error of 1 m, λ=3.6 cm, ω (earth sidereal rate)= 7.272×10^{-5} rads s^{-1}, the residual fringe rate (i.e. 1/time for a complete turn of phase error) $\approx$ 2 mHz.

Errors in celestial coordinates can arise from:

1. Observing a source with a poorly-known position, possibly determined from a lower resolution radio survey (e.g. VLA observations of 10-100 mas accuracy), or from optical observations, which might be affected by systematic differences between optical and radio frames at the 0.1 arcsec level.

2. Using an inadequate model of the precession/nutation of the earth's rotation axis. The residual fringe rate due to a position error $\Delta\theta$ is of order $\omega\Delta\theta\vec{B}_\lambda$, where $\vec{B}_\lambda$ is the baseline length in wavelengths; e.g. for a position error $\Delta\theta$=100 mas, $\vec{B}_\lambda$=2000 km, λ=3.6 cm, the residual fringe rate $\approx$ 2 mHz.

There can also be errors in aligning the terrestrial and celestial coordinate systems due to inaccurate knowledge of time. These epoch errors Δt can arise from systematic clock offsets and short-term variations in earth's rotation rate, which are usually measured as short-term UT1-UTC errors ($\approx$ 0.1ms). Epoch errors are generally equivalent to position errors of order $\Delta\theta = \omega\Delta t\vec{B}_\lambda$, e.g. Δt=10 ms, $\vec{B}_\lambda$=2000 km, λ=3.6 cm, the residual fringe rate $\approx$ 3 mHz.

17.1.2 Instrumental Errors

Instrumental phase errors are those errors introduced at the antenna due to propagation through the antenna optics and electronics before the sampled electric field is recorded onto tape. The primary source of instrumental phase errors are the independent frequency standards (clocks) used at each antenna. These VLBI frequency standards generate the local oscillator (LO) signals with which the radio frequency signals are mixed (see chapter 5) and synchronize the antenna time-keeping systems. Small differences between clocks on a baseline introduce phase errors into the visibility data. This source of phase error is unique to VLBI, since for CE arrays a common frequency standard is normally used for all antennas. VLBI clocks are typically accurate to a few μs and have rates $\approx 10^{-12}$ s s^{-1}, e.g. at λ=3.6 cm, this clock rate corresponds to a residual fringe rate = 0.8 mHz.

Another source of instrumental phase error is the axis-offsets between the rotation axes of antennas. These offsets lead to a varying path length to the phase center of the antenna of order H cos(elevation) for an alt-az mount, where H is the axis offset distance (Sovers 1991); the baseline phases reflect the time-varying difference between the elevation angles of two antennas. As an example, the VLBA axis offset is 2.35 m, typically this implies the signal path length changes by 2.35 m in 6 hours, i.e. 1.5 mHz at λ=3.6 cm.

Instrumental phase errors can also arise due to structural changes in the relative separation of dish components (e.g. dish and sub-reflector) due to changing gravitational stresses as the antenna tracks the source. Environmental factors (e.g. temperature/humidity changes) can also lead to varying electrical path delays in cables and/or electronics. Both these effects can be of order $\approx$ mm-cm. Note that many of the effects which depend on the azimuth and elevation of the antenna are not important for CE arrays where the antenna orientations are virtually the same.

17.1.3 Neutral Atmosphere Effects

Both water vapor and air have refractive indices $n \neq 1$, giving an increase in the effective path length along the line of sight to the source. It is convenient to consider the atmosphere above each antenna as having a quiescent "static" component whose refractivity n changes only with altitude upon which are superimposed stochastic variations in n (mainly due to variations in water vapor density) which may move rapidly over the antenna (the "dynamic" component).

The effect of the static component is to add a path length of $l_z m(z)$ where l_z is the path delay at the zenith and $m(z)$ is a "mapping" function which depends on zenith angle z (e.g. $m(z) \approx 1/\cos(z)$ at low and moderate z). Static troposphere effects are much more significant for VLBI than for CE arrays as both l_z and z can be quite different at each antenna.

The zenith delay l_z can be estimated from surface measurements using for-

mula such as the Saastamoinen model (Rönnäng 1989) which is

$$l_z = 0.228 \left[P_o + P_w \left(\frac{1255}{\mathrm{T}} + 0.05 \right) \right] f^{-1}(\lambda, h) , \qquad (17.2)$$

where l_z is measured in cm, P_o and P_w are the total pressure and the partial pressure due to water vapor at the surface respectively (in mb), T is the surface temperature (in degrees Kelvin) and f is a parameter close to unity which takes into account the variation of gravity with latitude λ and with height above the earth's geoid, h. The dry component of the path delay (i.e. the part which depends only on P_o) contributes $\sim$ 2.3m to L_z but can usually be estimated by the above formula to an accuracy of $\approx$ 0.05 cm (Davis et al. 1985). In contrast the wet component contribution can only be estimated via such ground measurements to an rms accuracy of about 2 cm (Elgered 1982). Use of water vapor radiometers appears to improve the accuracy of the wet-path estimates by factors of 2 or 3 (Rönnäng 1989). Provided that $z < 80°$, relatively good models of $m(z)$ exist and hence below these zenith angles the residual phase errors due to the static troposphere will be determined by the inaccuracies in estimating the zenith wet path delay.

The phase errors due to the static component depend only on zenith angle (and the slowly changing l_z) and are therefore smoothly varying in time. In contrast the dynamic component can give rise to rapidly varying random phase errors above each antenna. The dynamic component of the troposphere is normally modeled as being due to a "frozen screen", in which turbulence which extends up to an atmospheric scale height of L is blown over each antennas at a velocity of v $\sim$10 m s^{-1}. The spectrum of fluctuations in the screen is characterized by a structure function

$$D(b) = \left\langle [\phi(x) - \phi(x+b)]^2 \right\rangle , \qquad (17.3)$$

where $\phi(x) - \phi(x+b)$ is the difference in phase through the screen at two points separated by a distance b, and where the angle brackets refer to an ensemble average. Both theory and observations (Treuhaft and Lanyi 1987; Sramek 1990) suggest that for $b < L$ we have $D(b) = 1.4 \left(\frac{2\pi}{\lambda}\right)^2 {C_n}^2 L b^{5/3}$, while for $b > L$ we have $D(b) = 0.9 \left(\frac{2\pi}{\lambda}\right)^2 {C_n}^2 L^2 b^{2/3}$. Here C_n is a parameter describing the strength of the turbulence; typical C_n values are 1.6-1.8$\times 10^{-7}$ m$^{-1/3}$ (daytime, summer), and 0.6$\times 10^{-7}$ m$^{-1/3}$ (night, winter). Observed C_n values are generally within a factor of 2 of these median values 95% of the time (Sramek 1990).

17.1.4 Ionospheric Effects

The ionosphere is a region of free electrons and ions, permeated by geomagnetic fields, distributed in several layers from 60 to 10000 km above the earth's surface. Passage of a radio wave through the ionosphere causes additional phase/group delays, and Faraday rotation of the plane of polarization of a linearly-polarized

wave. The excess zenith path (in meters) is (Thompson, Moran and Swenson 1986)

$$\ell_o \approx \frac{40.3}{\nu^2}\mathrm{TEC}\,, \tag{17.4}$$

where TEC is the total electron content (electron column density in units of m^{-2}) along the line of sight to the source and ν is measured in Hz.

We can also separate ionospheric effects into a static component which is smoothly varying and superimposed upon this background are dynamic irregularities. The zenith column densities of electrons can vary considerably depending on time of day, season and the solar cycle. At the solar maximum zenith TEC can range from greater than 5×10^{17} m^{-2} during the day to 1×10^{17} m^{-2} during the night, i.e. at 1.6 GHz, ℓ_o can vary from 8 m (daytime) to 1.6 m (nighttime). During the solar minimum TECs are about a factor 5–10 less than these values. For VLBI observations the local time of day and source elevation at each antenna can be very different, therefore static ionospheric errors are a very significant source of phase error.

There are several methods of estimating and reducing the effects of the ionosphere:

1. We can use published ionospheric models, using parameters such as sunspot numbers, time of day, season etc. Although reasonably good at predicting the mean properties of the ionosphere such models are very poor at predicting daily TEC (i.e. errors can be as high as 40–50% of the total (Brown et al. 1991; Reilly et al. 1991);

2. We can directly measure the TEC using satellite observations of Faraday rotation combined with models of the earth's magnetic field (Gwinn 1990);

3. If the source is strong enough we can use measurements of the group delay at widely separated frequencies to estimate ionosphere TEC (i.e. S/X methods, see chapter 19).

Dynamic ionospheric effects are mainly due the passage of acoustic-gravity waves through the upper atmosphere leading to significant variations in TEC. Most important for radio observations are Medium-scale Travelling Ionospheric Disturbances (MSTIDs) which have horizontal speeds of 100–300 m s^{-1}, periods of 10-60 min, and wavelengths of several hundred km. The typical amplitude ΔTEC is of order $\approx 10^{15}$ m^{-2} (1% of daytime TEC). The origin and climatology of MSTIDs are still unclear although there are a number of possibilities (Van Velthoven 1990). Since the wavelengths of MSTIDs are much larger than typical CE array baselines, these ionospheric waves only affect the very lowest observing frequencies. For VLBI observations, the passage of a MSTID over one antenna can introduce significant phase errors.

17.2 Phase-Referencing

In conventional VLBI imaging we attempt to estimate and remove the effects of the large phase errors, delays and delay rates present in the data using the target data itself (i.e. global fringe-fitting/self-calibration). We search for these three unknowns over a solution interval set by the period over which the phase and its derivatives sufficiently characterize the phase errors (e.g. about 10 minutes at cm wavelengths). The methods for solving for these three unknowns are described in chapter 10. After removing the effects of the delays and delay-rates, we generally improve the estimation of the phases using an iterative scheme involving self-calibration and imaging (see chapter 13). Such schemes involve searching for a signal in a large multi-dimensional space using only a small interval of data, and in order to avoid confusion with a noise spike the signal must have a large SNR. For this reason such techniques only work for relatively bright objects. Furthermore since all the parameters are estimated assuming they are antenna-based all information about the absolute position of the source is lost.

Instead of using the target source itself to estimate phase errors it is possible to use an external calibrator source to calibrate the phase data. This technique, known as phase calibration to users of CE arrays, involves regular observations of a nearby calibrator to determine phase corrections to be applied to the target visibility data. Due to the large and rapidly changing phase errors in VLBI observations, we use the calibrator observations to determine delay-rate (phase derivative with time) and delay (phase derivative with frequency) as well as the instantaneous phase error at the central observing frequency; when applied to VLBI data, we refer to this technique as phase-referencing.

Let us examine the phase-referencing process in more detail. Imagine a weak target source of poorly-known position and structure located adjacent to a bright calibrator source. Let us also assume that we interleave observations of the target and the calibrator source. At times corresponding to the calibrator observations we can derive, via fringe-fitting to the bright calibrator, estimates of delay, delay-rate and phase. After interpolating and smoothing over time the calibrator delay solutions will generally provide good enough estimates of the target source delays to allow integration of the target (and calibrator) data over frequency without loss of coherence.

Having averaged the target and calibrator data to a single frequency channel the next step is to interpolate the calibrator phases over time and remove their effects from the target source data. Consider target observations at time t_2 sandwiched between calibrator observations at t_1 and t_3. The measured phases for the calibrator $\phi_{\rm cal}$ and target $\phi_{\rm targ}$ will be

$$\begin{aligned}
\phi_{\rm cal}(t_1) &= \phi_{\rm c}(t_1) + \phi^{\rm c}_{\rm inst}(t_1) + \phi^{\rm c}_{\rm pos}(t_1) + \phi^{\rm c}_{\rm ant}(t_1) + \phi^{\rm c}_{\rm atmo}(t_1) + \phi^{\rm c}_{\rm iono}(t_1) \\
\phi_{\rm targ}(t_2) &= \phi_{\rm t}(t_2) + \phi^{\rm t}_{\rm inst}(t_2) + \phi^{\rm t}_{\rm pos}(t_2) + \phi^{\rm t}_{\rm ant}(t_2) + \phi^{\rm t}_{\rm atmo}(t_2) + \phi^{\rm t}_{\rm iono}(t_2) \\
\phi_{\rm cal}(t_3) &= \phi_{\rm c}(t_3) + \phi^{\rm c}_{\rm inst}(t_3) + \phi^{\rm c}_{\rm pos}(t_3) + \phi^{\rm c}_{\rm ant}(t_3) + \phi^{\rm c}_{\rm atmo}(t_3) + \phi^{\rm c}_{\rm iono}(t_3) .
\end{aligned} \tag{17.5}$$

We have separated the geometrical phase errors into errors due to source positions and antenna positions, i.e. $\phi_{\rm geom} = \phi_{\rm pos} + \phi_{\rm ant}$, and $\phi^{\rm c}_{\rm atmo}$, $\phi^{\rm t}_{\rm atmo}$, $\phi^{\rm c}_{\rm iono}$ and $\phi^{\rm t}_{\rm iono}$ are the atmospheric/ionospheric phas errors towards the calibrator and target sources respectively. There are several ways to estimate the calibrator phase at time t_2 using the measured calibrator phases and phase-rates at times t_1 and t_3, usually involving forward and backward integration of the derived phase rates. Experiments using phase-referenced VLBA data suggest only small differences between the various schemes (Beasley et al. 1995).

We can represent the interpolated calibrator phase $\phi_{\rm cal}$ at time t_2, by

$$\tilde{\phi}_{\rm cal}(t_2) = \tilde{\phi}_{\rm c}(t_2) + \tilde{\phi}^{\rm c}_{\rm inst}(t_2) + \tilde{\phi}^{\rm c}_{\rm pos}(t_2) + \tilde{\phi}^{\rm c}_{\rm ant}(t_2) + \tilde{\phi}^{\rm c}_{\rm atmo}(t_2) + \tilde{\phi}^{\rm c}_{\rm iono}(t_2)\,, \tag{17.6}$$

where interpolated quantities are indicated by tildes. Differencing the target and interpolated calibrator phases (dropping the t_2 notation) the difference phases will be

$$\begin{aligned}\phi_{\rm targ} - \tilde{\phi}_{\rm cal} = (\phi_{\rm t} - \phi_{\rm c}) + (\phi^{\rm t}_{\rm inst} - \tilde{\phi}^{\rm c}_{\rm inst}) + (\phi^{\rm t}_{\rm pos} - \tilde{\phi}^{\rm c}_{\rm pos}) + (\phi^{\rm t}_{\rm ant} - \tilde{\phi}^{\rm c}_{\rm ant}) \\ + (\phi^{\rm t}_{\rm atmo} - \tilde{\phi}^{\rm c}_{\rm atmo}) + (\phi^{\rm t}_{\rm iono} - \tilde{\phi}^{\rm c}_{\rm iono})\,.\end{aligned} \tag{17.7}$$

At this point we can make some reasonable approximations: (a) $\phi^{\rm t}_{\rm inst} \approx \tilde{\phi}^{\rm c}_{\rm inst}$, i.e. the clocks error and electrical path delays effect both the target and calibrator data equally; (b) *isoplanarity*: that the target and calibrator are close enough together on the sky so that atmospheric/ionospheric phase errors are approximately the same along both lines of sight (i.e. assuming they are within the same isoplanatic patch), so that $\phi^{\rm t}_{\rm atmo} \approx \tilde{\phi}^{\rm c}_{\rm atmo}$ and that $\phi^{\rm t}_{\rm iono} \approx \tilde{\phi}^{\rm c}_{\rm iono}$; (c) for a small target-calibrator separation the effects of geometrical errors such as antenna position errors will also be approximately the same for target and calibrator, $\phi^{\rm t}_{\rm ant} \approx \phi^{\rm c}_{\rm ant}$; and (d) if the calibrator source is very compact we can assume that $\phi_{\rm c} = 0$. More generally we can image the bright calibrator source using self-calibration and correct the difference data for the calibrator *structure phase*, $\phi_{\rm c}$. Assuming we do this, then making use of the approximations described above we obtain;

$$\phi_{\rm targ} - \tilde{\phi}_{\rm cal} = \phi_{\rm t} + (\phi^{\rm t}_{\rm pos} - \tilde{\phi}^{\rm c}_{\rm pos}) + \text{interpolation errors}\,, \tag{17.8}$$

i.e., after correcting for calibrator structure, the phase-referenced difference phase contains only information about the target source structure and the positions of the target and calibrator source. Assuming negligible interpolation errors and a suitable calibrator, on Fourier inverting and deconvolving (CLEANing) the phase-calibrated target source data we should produce a good image of the target source.

Figure 17.1 on the facing page shows an example of phase-referencing for the source pair 1638+398/1641+399 (Beasley et al. 1995); in figure 17.1(*a*) the

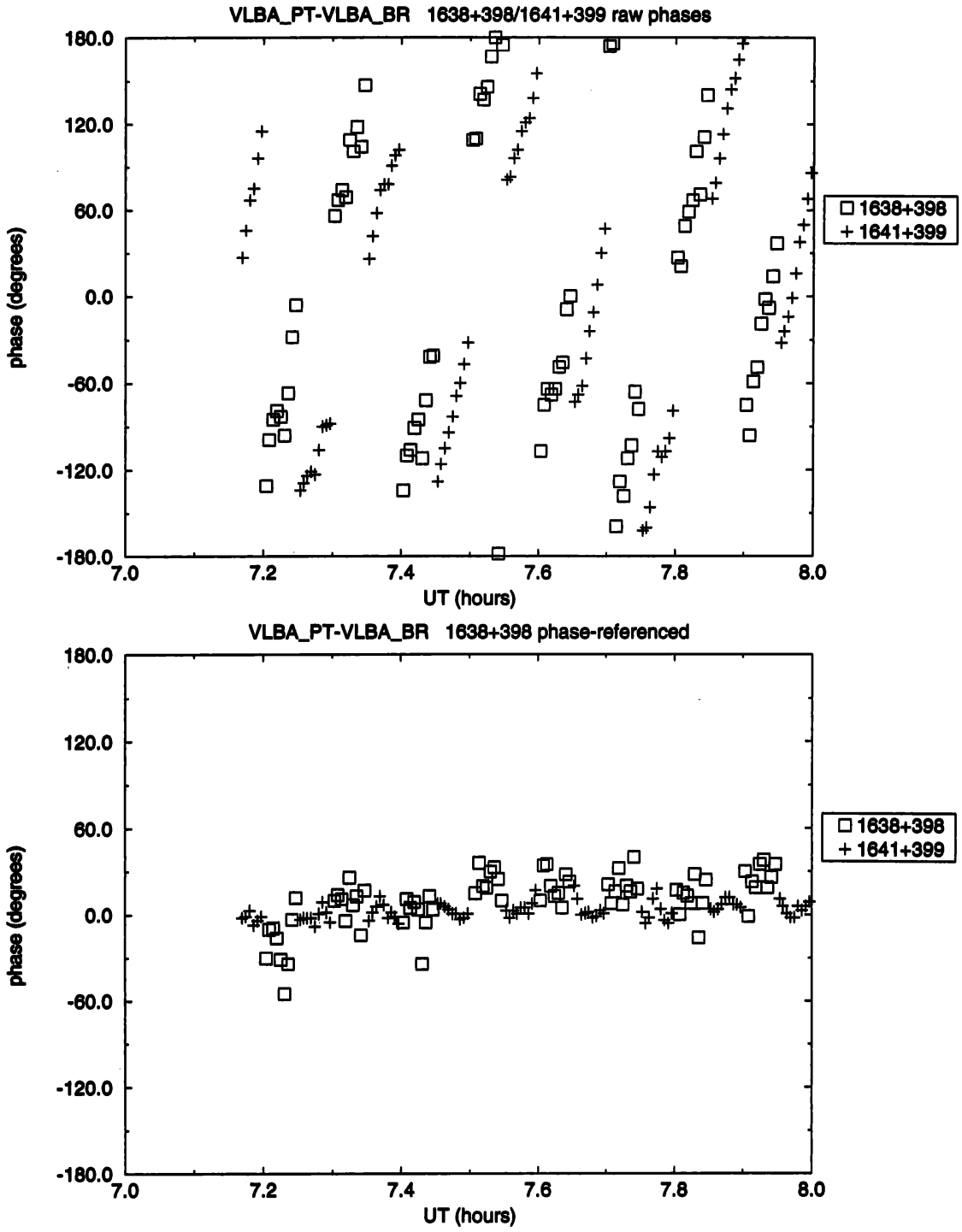

Figure 17.1: VLBA phase-referencing observation. *(a, top)* shows the raw phases on the sources 1638+398/1641+399; *(b, bottom)* shows the calibrated phases after fringe-fitting 1641+399 and phase-referencing the 1638+398 data.

raw phases are shown for a single baseline, while in (*b*) we see the phases of 1641+399 after fringe-fitting, and the phases of 1638+398 after interpolating the 1641+399 delay and delay-rate corrections. The implied coherence time for the phase-referenced 1638+398 visibilities is > one hour.

17.3 Imaging

17.3.1 Residual Phase Errors

Inevitably after phase-referencing there will be some level of residual phase errors due to inaccurate interpolation. In this section we discuss the effect of such phase errors on imaging quality. We will refer to the process of direct imaging, i.e. Fourier transformation of the (u, v) data followed by deconvolution (CLEANing); this form of phase-referenced imaging has been demonstrated by Alef (1989a) and Lestrade (1991). We will assess image quality using the dynamic range D, which we define as the peak response in an image divided by the largest negative sidelobe for a point source.

The size of the errors in the difference phase, and hence the dynamic range limit in the resultant image, will depend on four factors; (a) the quality of the a priori phase calibration applied to the target and reference source data, (b) the accuracy of the temporal interpolation of phase between calibrator observations (temporal phase errors), (c) the extent to which the phase errors in the direction of the calibrator mimic those in the direction of the target (angular phase errors), and (d) the accuracy of the phase calibrator position used at correlation.

17.3.2 A Priori Phase Calibration

The magnitude of phase errors in VLBI data demand good a priori phase calibration before successful phase-referencing. The a priori calibration model should incorporate all the available meteorology information, earth orientation parameters, ionospheric model etc. Since better estimates of these variables are often available after correlation it is usually best to reapply an improved delay model by adding back the effect of the recorded correlator model and removing a new total-delay model. The level of accuracy that can be achieved by such modeling has been extensively discussed in section 17.1 on page 328.

17.3.3 Temporal Phase Variations and Switching Time

Instrumental and geometrical phase errors vary relatively smoothly in time and so have little influence on setting the switching cycle time τ_s (defined as the time interval between the center of successive calibrator observations) or the achievable dynamic range. These parameters are instead set by the randomly varying tropospheric and ionospheric phase errors. In practice the main requirement on the switching time is that any change in atmospheric/ionospheric phase over this

interval must be much less than half a turn i.e. that over the switching interval the path length must change by much less than $\lambda/2$. If this condition does not hold there can be ambiguities in connecting the phase between successive calibrator observations. In other words, there can be problems of **phase connection**: of correctly connecting phase between observations without extra 2π turns of phase. Without reliable phase connection it is not possible to produce a useful image of the target source.

At frequencies > 1.6 GHz the dynamic troposphere will usually be the determining factor on setting the switching time. Treuhaft and Lanyi (1987) introduced structure function analyses of fluctuating tropospheric delay (see section 17.1 on page 328), which can be used to derive two critical switching times (Conway and Vermeulen 1995). Using the requirement that the rms path variation between calibrator scans is $< \lambda/4$, which should allow phase-connection in 95% of cases, then:

$$\tau_s(\max) = 25\lambda^{6/5}\cos^{3/5}(z)\,C_n^{-6/5}\,v^{-1} \qquad (17.9)$$

$$\tau_s(\max) = 100\lambda^{3}\cos^{3}(z)\,C_n^{-3}\,v^{-1} \qquad (17.10)$$

where τ_s is in minutes, λ is in cm, z is the zenith angle, C_n is in units of 10^{-7} $m^{-1/3}$ (and is typically about 2×10^{-7} $m^{-1/3}$) and v (ms^{-1}) is the turbulence screen velocity (typically about 10 ms^{-1}). The two timescales correspond to the cases when $\tau_s < L/v$ and $> L/v$, where L is the scale height of troposphere ($L/v \approx$ 100–200s). The switching time used should be smaller than the larger of the expressions. For example, for λ=6 cm, a zenith angle of 80°, poor tropospheric conditions ($C_n = 3.6 \times 10^{-7}$ $m^{-1/3}$), the critical switching time can be as small as $\approx$ 2 min.

At low frequencies, dynamic tropospheric effects are minimal while ionospheric effects (such as MSTIDs) become more important, limiting τ_s to $\leq$10 minutes in a majority of cases at frequencies below $\sim$1 GHz.

17.3.4 Angular Phase Variations and Switching Angle

The effects of errors in the estimation of atmospheric/ionospheric delays limit the angular distance between the calibrator and target sources (referred to as the switching angle θ_s). First let us consider the effects of the *static* component of the troposphere. In section 17.1 on page 328 we described the residual phase errors that arise in single source data due to inaccuracies in estimating the tropospheric zenith delay. Phase-referencing will reduce these single source phase errors by a factor of order the separation angle θ_s, where θ_s is measured in radians, hence the residual phase errors are linearly dependent on the target-calibrator separation. Numerical simulations suggest that for the VLBA the dynamic range limit due to uncertainties in the zenith troposphere is given approximately by (Conway and Vermeulen 1995);

$$D \approx 25\,\theta_s^{-1}\,(\Delta l/\lambda)^{-1}, \qquad (17.11)$$

where Δl is the error in the zenith delay estimate, θ_s is the target-calibrator separation in degrees. As an example if $\theta_s = 2°$, $\Delta l = 2$ cm (see section 17.1), $\lambda = 3.6$ cm then $D \approx 23$. Although the *dynamic* component of the troposphere moves rapidly across the antennas and hence limits the switching time, it has a negligible effect on the maximum target-reference separation as the atmospheric cells containing air of significantly different refractivity subtend relatively large angles.

The *static* ionosphere will also contribute phase errors which depend linearly on the target-calibrator separation. Numerical simulations (Conway and Vermeulen 1995) show that an upper limit to the achievable dynamic range is given approximately by

$$D \approx 30\nu\theta_s^{-1}(\Delta I)^{-1}\,, \tag{17.12}$$

where ΔI is peak daily residual TEC (in units of 10^{17} m^{-2}) and ν the observing frequency (in GHz). For example, at nighttime during solar maximum, using $\theta_s = 2°$, $\nu = 8.4$ GHz, and assuming no correction for ionospheric effects, the dynamic range D ≈ 25.

In contrast to the tropospheric case, at low frequencies the *dynamic* component of the ionosphere can be a limiting factor on the switching angle. Coherent quasi-sinusoidal phase variations due to MSTIDs have been seen both at 5 & 1.6 GHz (Conway and Vermeulen 1993; Beasley et al. 1995). In both cases there is evidence that the size of the phase errors increase significantly with increasing target-reference separation. At frequencies of 5 GHz and higher they are unlikely to be a significant problem, e.g. if $\theta_s = 2°$ then even the strongest MSTIDs (which might occur only 5% of time) will only limit $D \sim 50$. In contrast at 1.6 GHz the same MSTID will limit $D \approx 10$. For low frequency observations it might therefore be necessary to monitor ionospheric conditions (using ionosonde or satellite data) and avoid periods of bad ionospheric seeing.

17.3.5 Calibrator Position Errors

As shown in equation 17.8, errors in the assumed positions of the target and calibrator will contribute a term $(\phi^t_{pos} - \tilde{\phi}^c_{pos})$ to the difference phase. To first order the effect of this term will be to shift the phase-referenced image by an amount which depends only on the error in the *relative* separation between target and reference source. However it can be shown (Conway and Vermeulen 1995) that the phase contribution due to calibrator position errors cannot be exactly mimicked by a shift in the phase-reference image, as there will be additional phase offsets introduced which will limit the dynamic range. Although declination dependent, simulations suggest that

$$D \approx 500\Delta\theta^{-1}(\delta\theta/\theta_b)^{-1}\,, \tag{17.13}$$

where $\Delta\theta$ is the target-reference separation in degrees, and $\delta\theta$ and θ_b are the calibrator position error and interferometer resolution respectively. For a

$\delta\theta$ = 10 mas position error at 8.4 GHz and a $\Delta\theta = 2°$ separation, $D = 25$, therefore calibrator position errors can significantly limit the dynamic range of direct imaging.

17.3.6 Hybrid Self-Calibration Imaging

Given all sources of residual phase error described in the previous sections, particularly the angular phase errors due to the static troposphere and ionosphere, it will probably be difficult at centimeter wavelength to achieve dynamic ranges higher than 25 via direct imaging. This dynamic range limit means that for the full-track VLBA observations at centimeter wavelengths we can only obtain noise limited images for sources weaker than about 3 mJy.

Up until now we have only considered phase-referencing as a means of calibrating the phase of the visibility data which is then Fourier inverted and deconvolved (CLEANed) (i.e. we have considered only direct imaging). There is an alternative way of viewing phase-referencing—as a means of increasing phase coherence time and reducing the number of parameters that need to be estimated from the data—allowing self-calibration techniques to be applied to much weaker sources.

Using standard fringe-fitting/self-calibration techniques we must solve for delay, delay-rate and phase using only a small interval of data (i.e. ten minutes). After phase-referencing the minimum flux density required by such techniques is much reduced. First, in the process of phase-referencing, the target source data is averaged coherently over frequency, removing the need to search for a delay. Secondly after phase-referencing the residual temporal phase variations are reduced sufficiently so that there is also no need to solve for delay-rates, leaving only phase errors to be estimated. The solution intervals for self-calibration can be extended up to the coherence time of the phase-referenced data (defined as the time for phase to change by one radian), which can be as long as an hour or so. Empirically we have found in VLBA test observations (Beasley et al. 1995) that at 8.4 GHz, coherence times $\geq$1 hr were obtained $\approx$ 100% of the time for a 1.9° switching angle and 50% of the time for a 8.9° switching angle. At 1.6 GHz, coherence times of $\approx$ 20–30 min were obtained 66% of the time using a 1.9° separation and 50% of the time at 8.9°, with a coherence time $\gg$1 hr obtained 100% of the time for a 0.3° switching angle.

Conway and Vermeulen (1995) have made a theoretical analysis of the regimes in which direct imaging and hybrid self-calibration methods can be used. The major conclusion, broadly consistent with the empirical results, is that if the zenith delay error $< 3\lambda$, then for a 2° switching angle, techniques exist to obtain noise limited images of sources of any flux density. For sources with compact structure with flux density >10-20 mJy we can use standard self-calibration techniques, e.g. fringe-fitting; for sources between 3 mJy and 10 mJy hybrid self-calibration using long solution intervals will give thermal-noise-limited images; and for sources < 3 mJy direct imaging will give thermal-noise -limited images.

17.4 Relative Astrometry

As shown by equation 17.8 the phase-referenced phase is sensitive to the positions of both the target and reference; to first order it can be shown that the phase-referenced phase depends on the relative separation of the two sources.

One way to measure this relative separation is to image the phase-calibrated target source data and find the position of the target source relative to the image center (Lestrade 1991). From this position offset and the assumed positions of target and reference used at correlation the relative positions of target and reference can be found. This technique has been used to measure the position of the star Algol (3 mJy) relative to a background extragalactic source with an accuracy of 0.5 mas (Lestrade 1991).

Alternatively, one can directly search for a relative separation between target and reference which directly fits the observed variation in difference phase as a function of time. A handicap is that the phase is only recorded modulo 2π. However for pairs of strong sources ambiguities of 2π in the difference phase can be recovered by using observed delays and delay-rates for the target and reference sources. Such techniques have been used to measure the relative separation of 3C 345 and NRAO 512 to an accuracy of 0.3 mas (Shapiro et al. 1979), and the relative separations of 4 pairs of extragalactic sources to a very high accuracy (50μas) for source separations 0.5–4° (Marcaide and Guirado 1993). More details on the technique of differential astrometry can be found in chapter 19.

17.5 Prospects For Phase-Referencing

The success of phase-referencing at any given frequency depends in part on whether, given the constraints on switching interval (τ_s) and switching angle (θ_s), there exist suitable phase-calibrators. To be applicable to any part of the sky there must be a high probability of finding a suitable calibrator within the maximum switching angle. Such a calibrator should have a compact or simple structure, and must be detectable with high signal to noise (e.g. ideally $\gg 10$ over a time interval $< \tau_s/2$) on most baselines. In order to achieve high dynamic range the calibrator position should be known to a few beams, however tens of beams should be adequate for most purposes.

At 5 & 8.4 GHz (and possibly 15 GHz) prospects for phase-referencing are excellent. As described earlier, even given the expected limitations on a priori calibration it should be possible to produce noise limited images using target-reference separations of $2° - 3°$ and perhaps larger. Both theory and observations suggest a switching cycle of 6 minutes is ample for phase connection under typical atmospheric conditions. The list of flat spectrum sources being compiled for MERLIN phase-referencing (Patnaik et al. 1992), which are flat spectrum, compact, have 5 GHz flux density $S_{5GHz} \geq 200$ mJy, and will eventually cover the declination range $-30° < \delta \leq 90°$ will provide an adequate sample of potential VLBI calibrator sources. Previous experience with VLBI imaging

at 5 GHz (Pearson and Readhead 1988) suggests that the vast majority of these sources ($> 95\%$) should prove compact enough to use as calibrators at 5 & 8.4 GHz. Other potential sources are compact sources selected from the VLBI literature, e.g. geodetic lists or VLBI structure surveys (Ma et al. 1990; Pearson and Readhead 1988; Preston et al. 1985; Russel et al. 1992; Wilkinson et al. 1993); note that the position accuracy of these sources may be insufficient for high dynamic-range imaging (see section 17.3 on page 336). A VLBA calibrator survey is underway, which will provide a grid of compact sources with milliarcsecond-precision positions suitable as VLBI phase calibrators (Beasley, in preparation).

At low frequencies (≤ 1.6 GHz) the maximum switching angle may be limited by ionospheric effects such as MSTIDs (see section 17.3.5). Under bad conditions, to achieve good dynamic range (i.e. ≈ 30) it may be necessary to use separations $< 2°$. This means either using weaker (i.e. more numerous) calibrators, or monitoring ionospheric conditions and only observing under good conditions. At the lowest frequencies (e.g. 327 MHz) bright, compact extragalactic sources appear to be relatively rare, although pulsars observed in a "gated" mode may be a suitable alternative.

At high frequencies (22 and 43 GHz) full phase-referencing may prove to be very difficult. To allow phase-connection the switching times at these frequencies need to be fast (i.e. < 60s); this short switching interval combined with the high system temperatures at these frequencies means that calibrators must be brighter than about 500 mJy. Furthermore, even to achieve a dynamic range of 10 using direct imaging at 22 GHz requires (see eqn. 17.11) a source separation of less than 1°. Added to this is the problem of finding suitably compact calibrators at these frequencies. It appears that there are likely to be an insufficient number of bright calibrators to cover the whole sky. More limited forms of phase-referencing in which external calibrators are used only to determine delays and delay-rates (i.e. delay/rate referencing) will however still be applicable.

17.6 Summary and Conclusions

Phase-referencing can be used to increase image sensitivity and dynamic range, and enable accurate differential astrometry, using regular switching between the target source and a nearby (~degrees) calibrator to derive delay, rate and phase corrections to interpolate to the target visibilities. Successful phase-referencing depends on phase-connection of the calibrator observations, and minimizing residual errors due to angular variations in phase. In many cases phase-referencing allows us to achieve thermal-noise-limited images at (potentially) sub-mJy flux densities. This ability has enormous astronomical potential, including the imaging of radio-quiet quasars, radio stars, weak AGNs, astrometry and pulsar proper-motions.

References

Alef, W. 1989. "Introduction to phase reference mapping". See Felli and Spencer (1989), p. 261.

Baldwin, J. E., & Wang, Shouguan (Eds.) 1990. *URSI/IAU Symp. on Radio Astronomical Seeing.* Beijing: International Academic Publishers.

Beasley, A. J., *et al.* 1995. "Tropospheric measurements with the VLBA". In preparation.

Brown, L. D., Daniell, R. E., Fox, M. W., Klobuchar, J. A., & Doherty, P. H. 1991. "Evaluation of six ionospheric models as predictors of total electron content". *Radio Sci.* **26**, 1007.

Conway, J. E., & Vermeulen, R. C. 1993. "VLBA phase-referencing tests". See Davis and Booth (1993), p. 409.

Conway, J. E., & Vermeulen, R. C. 1995. "Strategies for VLBA phase-reference imaging. I. Phase stability and dynamic range". In preparation.

Davis, J. L., Herring, T. A., Shapiro, I. I., Rogers, A. E. E., & Elgered, G. 1985. "Geodesy by radio interferometry: effects of atmospheric modelling errors on estimates of baseline length". *Radio Sci.* **20**, 1593.

Davis, R. J., & Booth, R. S. (Eds.) 1993. *Sub-Arcsecond Radio Astronomy.* Cambridge: Cambridge University Press.

Elgered, G. K. 1982. "Tropospheric wet path-delay measurements". *IEEE Trans. Ant. Prop.* **AP-30**, 502.

Felli, M., & Spencer, R. (Eds.) 1989. *Very Long Baseline Interferometry*, Volume 283 of *NATO ASI Series C.* Dordrecht: Kluwer.

Gwinn, C. R. 1990. "Comparison of ionospheric correction techniques for VLBI". See Baldwin and Wang (1990), p. 180.

Lestrade, J.-F. 1991. "VLBI phase referencing for observations of weak radio sources". In T. J. Cornwell and R. A. Perley (Eds.), *IAU Coll. 131, Radio Interferometry: Theory, Techniques, and Applications.* Volume 19 of *ASP Conference Series.* San Francisco: Astronomical Society of the Pacific.

Ma, C., Shaffer, D. B., De Vegt, C., Johnston, K. J., & Russel, J. L. 1990. "A radio optical reference frame. I. Precise radio source positions determined by Mark III VLBI: Observations from 1978 to 1988 and a tie to the FK5". *Astron. J.* **24**, 1284.

Marcaide, J. M., & Guirado, J. C. 1993. "High precision differential astrometry in large angular separation pairs of radiosources". In W. J. Tango and J. G. Robertson (Eds.), *IAU Symp. 158, Very High Angular Resolution Imaging.* Dordrecht: Kluwer, p. 445.

Patnaik, A. R., Browne, I. W. A., Wilkinson, P. N., & Wrobel, J. M. 1992. "Interferometer phase calibration sources—I. The region $35° \leq \delta \leq 75°$". *Monthly Notices Roy. Astron. Soc.* **254**, 655.

Pearson, T. J., & Readhead, A. C. S. 1988. "The milliarcsecond structure of a complete sample of radio sources. II. First-epoch maps at 5 GHz". *Astrophys. J.* **328**, 114.

Preston, R. A., Morabito, D. D., Williams, J. C., Faulkner, J., Jauncey, D. L., & Nicolson, G. D. 1985. "A VLBI survey at 2.29 GHz". *Astron. J.* **90**, 1599.

Reilly, M. H., Rhoads, F. J., Goodman, J. M., & Singh, M. 1991. "Updated climatological model predictions of ionospheric and HF progation parameters". *Radio Sci.* **26**, 1017.

Robertson, D. S., Carter, W. E., & Fallon, F. W. 1988. "Earth rotation from the IRIS project". In M. J. Reid and J. M. Moran (Eds.), *IAU Symp. 129, The Impact of VLBI on Astrophysics and Geophysics.* Dordrecht: Kluwer, p. 391.

Rönnäng, B. O. 1989. "Geodesy-VLBI observables". See Felli and Spencer (1989), p. 298.

Russel, J. L., Jauncey, D. L., Harvey, B. R., White, G. L., Reynolds, J. E., Ma, C., Johnston, K. J., Nothnagel, A., Nicolson, G., Kingham, K., Hindsley, R., de Vegt, C., Zacharias, N., & Malin, D. F. 1992. "A radio optical reference frame. III. Additional radio and optical positions in the southern hemisphere". *Astron. J.* **103**, 2090.

Shapiro, I. I., Wittels, J. J., Counselman, III, C. C., Robertson, D. S., Whitney, A. R., Hinteregger, H. F., Knight, C. A., Rogers, A. E. E., Clark, T. A., Hutton, L. K., & Niell, A. E. 1979. "Submilliarcsecond astrometry via VLBI. I. Relative position of the sources 3C 345 and NRAO 512". *Astron. J.* **84**, 1459.

Sovers, O. J. 1991. "Observation model and parameter partials for the JPL VLBI parameter estimation software "MODEST"—1991". JPL Publication 83-39, Rev. 4.

Sramek, R. A. 1990. "Atmospherical phase stability at the VLA". See Baldwin and Wang (1990), p. 21.

Thompson, A. R., Moran, J. M., & Swenson, G. W., Jr. 1986. *Interferometry and Synthesis in Radio Astronomy.* New York: Wiley-Interscience. First (1991) and second (1994) reprintings by Krieger Pub. Co., Malabar (Florida).

Treuhaft, R. N., & Lanyi, G. E. 1987. "The effect of the dynamic wet troposphere on radio interferometric measurements". *Radio Sci.* 22(2), 251.

Van Velthoven, R. F. J. 1990. *Medium Scale Irregularities in the Ionospheric Electron Content.* Ph. D. thesis, Technical University Eindhoven.

Wilkinson, P. N., Polatidis, A. G., Readhead, A. C. S., Xu, W., & Pearson, T. J. 1993. "The Caltech-Jodrell Bank VLBI survey". See Davis and Booth (1993), p. 213.